Simultaneous fat-referenced proton resonance frequency shift thermometry and MR elastography for the monitoring of thermal ablations

Kisoo Kim, Elodie Breton, Afshin Gangi, Jonathan Vappou

Title page:

Simultaneous fat-referenced PRFS Thermometry and MR Elastography for the monitoring of thermal ablations

Authors:

Kisoo Kim[1], Elodie Breton[1], Afshin Gangi[1,2], and Jonathan Vappou[1*]

Institution information:

[1]ICube - UMR7357, Université de Strasbourg, CNRS, Strasbourg, France

[2] Department of Interventional Imaging, Hôpitaux Universitaires de Strasbourg, Strasbourg, France

Running head: Simultaneous FRPRFS and MRE for the monitoring of thermal ablations

Key words: MR Thermometry; Fat referenced PRFS; MR Elastography; interventional MR; thermal ablation;

Word count: 2798

***Corresponding author :**

Jonathan Vappou, PhD

ICube, s/c IHU Strasbourg, 1 place de l'Hôpital, 67091 Strasbourg Cedex, FR

Email: jvappou@unistra.fr

Abstract

Purpose: Simultaneous fat-referenced proton resonance frequency shift (FRPRFS) thermometry combined with MR Elastography (MRE) is proposed in order to continuously monitor thermal ablations for all types of soft tissues, including fatty tissues. FRPRFS thermometry makes it possible to measure temperature even in the water fraction of fat-containing tissues while enabling local field-drift correction. MRE allows measuring the mechanical properties of tissues that are related to tissue structural damage.

Methods: A gradient-echo MR sequence framework was proposed that combines the need for multiple TE acquisitions for the water-fat separation of FRPRFS, and the need for multiple MRE phase-offsets for elastogram reconstructions. Feasibility was first assessed in a fat-containing gelatin phantom undergoing moderate heating by a hot water circulation system. Subsequently, High Intensity Focused Ultrasound (HIFU) heating was conducted in porcine muscle tissue ex-vivo (N=4; 2 samples, 2 locations /sample).

Results: Both FRPRFS temperature maps and elastograms were updated every 4.1 s. In the gelatin phantom, FRPRFS was in good agreement with optical fiber thermometry (average difference 1.2±1℃). In ex-vivo HIFU experiments on muscle tissue, the shear modulus was found to decrease significantly by 34.3±7.7 % (Exp.#1-Sample#1), 17.9±10.0 % (Exp.#2-Sample#1), 55.1 ±8.7 % (Exp.#3-Sample#2), and 34.7±8.4 % (Exp.#4-Sample#2) as a result of temperature increase (ΔT = 22.5±4.2℃, 14.0±2.8℃, 14.7±3.7℃, and 14.5±3.0℃, respectively).

Conclusion: This study demonstrated the feasibility of monitoring thermal ablations with FRPRFS Thermometry together with MRE, even in fat-containing tissues. The acquisition time is similar to non-fat referenced PRFS Thermometry combined with MRE.

1. INTRODUCTION

MR thermometry is commonly used to control heat deposition and to estimate tissue damage during MR-guided thermal ablations.[1–4] MR thermometry based on the water proton resonance frequency shift (PRFS)[5] is the most commonly used method because it offers high temperature sensitivity within the temperature range encountered during thermal ablations, and fast acquisition times in the order of a few seconds. However, fundamental limitations of PRFS thermometry need to be considered when applying this method for thermal ablation monitoring. First, PRFS temperature information provides temperature changes through the difference between the current phase and a baseline phase image. Hence, time-varying field drift and motion between successive scans can result in temperature errors, if not corrected for. Second, PRFS provides an instantaneous parameter, namely, temperature changes, which does not directly relate to tissue damage. The cumulative thermal dose (TD) represents an integration of temperature over time and has been shown to be a reliable marker of tissue damage.[6] However, fundamental limitations when using TD alone for monitoring thermal ablations over time need to be mentioned, such as the fact that TD thresholds are tissue-dependent[7], and that TD is particularly sensitive to any uncertainty or bias due to its cumulative property.[8] TD has also been shown to be poorly correlated to non-perfused volume (NPV), a reliable marker of post-ablation tissue damage, showing potential errors of MR Thermometry due to long-term heat accrual.[9] Third, PRFS thermometry in fat-containing tissues may result in significant temperature errors depending on echo time, fat fraction, and extent of temperature increase because the temperature dependent electron-screening constant in fat is negligible compared to the one of water protons.[10,11]

Fat-Referenced PRFS MR thermometry (FRPRFS)[12,13] using water-fat separation has been developed to tackle some of these limitations. The water-fat separation makes it possible to measure the temperature-induced PRFS from the phase of the water fraction contained in fatty tissues, and no longer from the global phase of mixed water and fat protons. Moreover, time-varying field drifts can be estimated from the phase of the fat fraction because, as previously mentioned, temperature induced changes are negligible in fat. Hence, water proton only PRFS temperature estimation can be obtained while correcting for time-varying field drifts in soft tissues, including fat-containing tissues.[13]

Recently, tissue elasticity has received increasing attention as a biomarker that would be complementary to temperature. Structural changes occurring during thermal ablations result in changes in tissue mechanical properties.[14–16] MR Elastography (MRE) offers the possibility to measure the mechanical properties of soft tissues non-invasively. While MRE is mostly used for diagnosis, this method has also been proposed as a tool for assessing thermal damage after an ablation.[14,17] Corbin et al.[18] proposed an interventional MRE protocol that allows for simultaneous PRFS temperature and elasticity monitoring at high frame rates (~0.5 Hz). More recently, Hofstetter et al. developed a novel MRE approach that relies on shear wave generation using acoustic radiation force pushes at multiple locations and composite

reconstruction, allowing for elasticity mapping. This method was used successfully to assess elasticity changes following High Intensity Focused Ultrasound (HIFU) ablation.[19]

All these studies have used conventional PRFS thermometry so that their use in fat-containing tissues may lead to significant errors in temperature estimation. The general objective of the proposed work is to extend the interventional MRE/MR Thermometry method to any type of soft tissues, including fat-containing tissues. For this purpose, a time-efficient strategy is proposed that allows for simultaneous FRPRFS thermometry and MRE. On one hand, an iterative least square fitting algorithm (IDEAL) is used for fast and robust water-fat separation.[20,21] The water and fat signal model is solved by using multiple TE datasets. On the other hand, MRE reconstructions require the acquisition of several images with varying phase-offsets between the mechanical wave and the motion sensitive gradients (MSG), in order to capture the shear wave at different propagation times. The strategy described here takes advantage of the acquisition of several phase-offsets in order to obtain the several echo times required for water-fat separation. Echo times and phase-offsets are jointly incremented to enable water-fat separation for FRPRFS thermometry along with MRE. The number of MRE phase-offsets and the number of TE used to solve the IDEAL algorithm are the same; hence, elastogram and FRPRFS temperature map are updated at the same time.

2. METHODS

2.1 Proposed framework

As shown in Fig.1a, a gradient-recalled echo (GRE) MRE sequence is modified in order to obtain varying echo times for water/fat separation: each pair of images with opposite MSG is acquired at a specific TE and its corresponding MRE phase-offset. The MRE phase-offset θ corresponds to the trigger delay between the mechanical shear wave and the MSG. The acquisition scheme (Fig.1b) consists of interleaved acquisitions with opposite MSG polarities (MSG$+/-$) and identical TE and phase-offset; hence, both TE and phase-offset are incremented every two images.

2.2 Image reconstruction

A 2D phase unwrapping algorithm[22] is applied to each phase image before reconstruction of elasticity and temperature maps. Different combinations of each pair of phase images acquired with opposite MSG polarities are used either for MRE elastogram reconstruction (difference) or for PRFS thermometry (average).[23] The first elastogram and temperature map are obtained once a full dataset including 4 phase-offsets / 4 TEs is obtained; subsequent ones can be reconstructed with every newly obtained pair of phase images with opposite MSG.[18]

2.2.1 Elasticity mapping

The subtraction of each pair of phase images acquired with opposite MSG polarities offers two positive outcomes in MRE: it doubles motion-encoded phase shifts while removing the background phase. Once 4 phase-offsets have been acquired, a temporal Fourier transform is applied to extract the fundamental MRE excitation frequency. A local frequency estimation (LFE)-based algorithm is used to estimate the local wavelength.[24] Finally, the shear modulus is calculated by $\mu = \rho(\lambda f)^2$ under the assumptions of linear elasticity and uniform tissue density (1000 kg/m^3).

2.2.2 Temperature mapping using the chemical shift water-fat separation

Each pair of phase images acquired with opposite MSG polarities is averaged in order to suppress the motion-dependent phase[23], while preserving the background phase including temperature information. The multiple TE datasets are used for temperature estimation. The measured signal can be expressed in terms of the water and fat components as follows:

$$S(TE_n) = \left(\rho_w + \rho_f \sum_{p=1}^{P} \alpha_p \cdot e^{-i2\pi f_p TE_n} \right) \cdot e^{-(R_2^* + i2\pi\Psi)TE_n} \quad [1]$$

Where $S(TE_n)$ is the complex signal of the nth echo time TE_n, ρ_w and ρ_f are the complex-valued water and fat signals, f_p is the difference of spectral peaks between fat and water (-3.8, -3.4, -2.6, -1.94, -0.39, and 0.6 ppm)[21] and α_p is the relative amplitude of each spectral peak (0.087, 0.694, 0.128, 0.004, 0.039, and 0.048)[21], R_2^* is the global transversal relaxation rate ($R_2^* = 1/T_2^*$), and Ψ is the off-resonance precession.

The IDEAL algorithm is used to solve Eq. [1] with an iterative approach.[20,21] Generally, the first step of the IDEAL processing consists in estimating the field map (R_2^* decay and Ψ) via the least square fitting error. Recently, the hierarchical IDEAL[20] method was proposed to estimate the field map by using a multiresolution technique, for improved computational efficiency. In this study, the hierarchical IDEAL is applied before heating in order to obtain a reliable estimate of the field map. Once the field map is identified, the second step consists in extracting the complex water and fat signals based on (R_2^* and Ψ) estimates.[20]

Temperature changes affect the water signal $\rho_w = \rho_w^0 e^{i\phi_T}$, where ϕ_T is the phase shift caused by temperature and ρ_w^0 is the water signal in the absence of temperature change. The field map is estimated once before the ablation to extract both water and fat complex signals. This approach aims at reducing the computational complexity during the ablation by avoiding the optimization step of the IDEAL algorithm.

This simplification is possible for two reasons. First, time-varying B_0 field drifts affect both the phases of water and fat; the effect of B_0 field drifts can therefore be estimated by a spatial polynomial fitting of the fat phase map in fat-containing tissues (field drift correction map), so that they are corrected for in the water phase map. Second, contrary to B_0 field drifts, temperature induced R2* changes are neglected because they only affect the magnitude of both water and fat signals, and hence have no effect on temperature estimates.

Therefore, temperature changes, ΔT (℃), can be estimated from the phase of water protons, with field drift correction, using FRPRFS, following[13]:

$$\Delta T = \frac{[\phi_w - \phi_w^0] - [\phi_C - \phi_C^0]}{\gamma \alpha B_0 TE} \quad [2]$$

Where ϕ_w and ϕ_w^0 are respectively the current and baseline water phase maps, ϕ_C and ϕ_C^0 are respectively the current and baseline field drift correction maps, γ is the gyromagnetic ratio of the hydrogen nuclei, B_0 is the main magnetic field, α is the temperature dependent water chemical shift (≈-0.01 ppm/℃), and TE is the average of the echo times used.

2.3 Experimental setup

All experiments were performed in a 1.5 T MRI (MAGNETOM Aera, Siemens Healthcare, Germany) using pneumatic MRE excitation. For monitoring during the ablation, images were transferred to a personal computer through TCP/IP connection and processed with Matlab (Mathworks, USA).

The proposed method was first demonstrated in a gel phantom experiment with hot water circulation, mimicking a thermal ablation in fatty tissues. The phantom was made of 8% gelatin in water and contained a water/fat cylindrical inclusion (2% gelatin in milk cream, 20% fat). A cylindrical plastic tube chamber connected to a water circuit was placed inside the inclusion for hot water circulation (Supporting information Figure S1). After baseline imaging for 100 s, hot water circulation was first activated between 100 s and 220 s, and a second time between 370 s and 417 s. The pneumatic MRE exciter was positioned below the phantom. Relevant acquisition parameters include: 4 TEs 8.2/9.7/11.2/12.7 ms; TR 16 ms; Flip angle 15°; FOV 300 mm × 300 mm; Matrix 128×128; Slice thickness 6 mm; Bandwidth 800 Hz/pixel; MSG frequency 162 Hz; mechanical wave frequency 125 Hz; MRE phase-offsets 4; Readout MSG encoding direction. Images were acquired in the axial plane, 5 mm away from the hot water tube in the head-foot direction. An optical fiber thermometer (LumaSense Technologies, USA) with 2 probes was used for reference temperature measurements. Field correction maps were obtained using a second order polynomial fitting of the fat phase in the cream.

Second, the proposed framework was used to monitor heating induced by HIFU in ex vivo muscle tissue (N=4). Two porcine rib muscle samples obtained from a local butchery were enclosed in a gel made of 2% gelatin in milk cream and covered with 7% gelatin (Supporting information Figure S2). For each sample, HIFU heating was performed at two different locations, leading to a total of N=4 experiments. A 128-element HIFU transducer (1 MHz central frequency, Imasonic/IGT, France) was positioned on the top of the tissue using a degassed water layer for acoustic coupling. The MRE acoustic exciter was placed below the container. The total scanning time was 10 minutes with successively 2 min baseline, 2 min HIFU heating and 6 min cooling period. HIFU ablation was performed using a 5-point focusing circular pattern (4 mm in diameter, 2 s/point) at an acoustic power of 45W. MR parameters identical to those used for the gel phantom experiment were used in sample 1 (experiments #1 and #2). Due to substantial differences in terms of tissue elasticity, the mechanical wave frequency was changed to 100Hz for sample 2 (experiments #3 and #4), yielding a different value of TR (20 ms); images were acquired in the sagittal plane, MSG encoding in slice direction.

3. RESULTS

3.1 Validation experiment in a gel phantom

Figure 2 shows temperature changes ΔT, elasticity changes $\Delta\mu$, elasticity maps μ and wave images measured at times 40 s (resting state), 200 s (first heating), and 400 s (second heating).

Temperature increase resulted in cream softening. Two ROIs (2×2 pixels) were selected at the tips of the optical fiber sensors. Time-dependent profiles of ΔT and $\Delta\mu$ measured in these ROIs are plotted in Fig. 3. Temperature changes measured with FRPRFS thermometry were in good agreement with those of the optical fiber sensors. The mean absolute difference in ROIs 1 and 2 were 1.5±1.3 ℃ and 0.9±0.7 ℃, respectively. Over the course of the experiment, the shear modulus was found to decrease from 21.6±1.2 kPa to 10.53±0.3 kPa in ROI 1, and from 20.6±0.7 kPa to 15.4±0.7 kPa in ROI 2.

3.2 Ex-vivo HIFU experiments

Because of high variability across the muscle samples, changes in mechanical properties are displayed in terms of relative stiffness changes (RSC= $\Delta\mu/\mu_0$, where μ_0 is the initial stiffness). Figure 4 shows ΔT, RSC, elasticity maps, and wave images measured before (100 s), after HIFU heating (250 s), and during cooling down (570 s) in one experiment. Shear modulus was found to decrease at the focal spot, as shown in the RSC maps.

ΔT and RSC were averaged within an ROI that was automatically computed as the region including all pixels exceeding 66.7% of the maximum peak temperature increase around the focal spot. Time-dependent profiles of ΔT and RSC for the four samples are plotted in Fig. 5. Shear moduli were found to decrease by 34.3±7.7 % (Exp.#1), 17.9±10.0 % (Exp.#2), 58.7±3.9 % (Exp.#3), and 36.7±6.7 % (Exp.#4) as a result of moderate temperature increase of 22.5±4.2℃, 14.0±2.8℃, 14.7±3.7℃, and 14.5±3.0℃ (Exp.#1-4).

4. DISCUSSION

Standard MRE sequences rely on image acquisitions at a single echo time for all MRE phase-offsets. In this study, the echo time TE is increased with each MRE phase-offset for FRPRFS thermometry. The proposed acquisition scheme keeps the acquisition time identical to previously developed combined PRFS thermometry and MRE.[18]

Several limitations of the MRE protocol should be discussed. First of all, MRE images are acquired with varying TEs, as a consequence of the IDEAL acquisition scheme. Because of T2* signal decay, this may cause variable phase-to-noise ratio between successive MRE images. In particular, the phase-to-noise ratio of long TE acquisitions may become critical in tissues with short T2*. As in conventional MRE, this limitation can be partially overcome by increasing the MSG frequency, thus shortening the TE, at the expense of the wave-to-noise ratio. Secondly, elastograms were reconstructed using the LFE algorithm under the assumption of linear elasticity. The LFE algorithm is commonly used in clinical studies thanks to its robustness. However, LFE methods may have lower spatial resolution and higher averaging effect than other reconstruction algorithms.[25] This may lead to errors in shear modulus estimates around the focal region, especially at the onset of elasticity changes, as the region where such changes occur is very limited in size. Accuracy could be improved by increasing shear wave excitation frequency, thus improving the MRE resolution. However, increasing excitation frequency affects shear wave penetration and may result in lower wave-to-noise ratio due to increased attenuation. Despite such potential limitations, the LFE algorithm is used in this study because its processing time is well suited for the monitoring of thermal ablations.

As seen in figures 4 and 5, rib muscle elasticity was found to be particularly heterogeneous. Such variability in muscle elasticity has already been observed[16] and may be related to variability in muscular fiber organization patterns. Because of such variations, results were presented in terms of relative changes of shear modulus. Similar behavior was found for the four samples tested: the shear modulus was found to decrease significantly as a consequence of moderate temperature elevation. This behavior has already been

reported previously by several teams. Wu et al. reported a decrease of bovine muscle shear modulus by almost 50% up to absolute temperatures of 60 °C ex vivo, followed by significant stiffening at higher temperatures. Similar trends were reported by Sapin et al.[16] and Arnal et al.[26] in ex vivo tissue. These studies suggest that muscle tissue softening occurring at moderate temperature elevation may be due to protein structure unfolding.[14,16]

Both phantom and rib tissue have relatively homogeneous water-fat distributions so that temperature-induced susceptibility changes in the fat might be slight in these experiments.[27,28] The FRPRFS measurement in the gel phantom experiment showed no significant difference when compared to optical fiber thermometry. Further study is needed to compensate for temperature-induced susceptibility changes in heterogeneous tissues.[27]

Finally, combining an external MRE exciter with interventional material (HIFU or percutaneous) may be particularly challenging in terms of spatial access. Translating this setup in vivo would certainly require using interventional-specific excitation strategies such as percutaneous vibrating needles[18] or the acoustic radiation force.[19] However, this investigation falls beyond the scope of this paper, which aims at demonstrating the feasibility of performing simultaneous FRPRFS MRT and MRE with IDEAL fat/water separation.

5. CONCLUSIONS

In this study, a new framework was developed for FRPRFS thermometry coupled with MRE for the monitoring of thermal ablations. This protocol was validated in a gel phantom and ex vivo in porcine muscle tissue. FRPRFS thermometry coupled with MRE has similar acquisition time as regular PRFS thermometry coupled with MRE, while providing refined temperature monitoring for thermal treatments in soft tissues.

ACKNOWLEDGMENTS

This work was partly funded by the French state funds managed by the ANR (within the Investissements d'Avenir programme for the Labex CAMI); Grant number: ANR-11-LABX-0004. We acknowledge the use of the Fat-Water Toolbox from the ISMRM Workshop on Fat-Water Separation 2012 (http://ismrm.org/workshops/FatWater12/data.htm).

REFERENCES

1. Parker DL. Applications of NMR Imaging in Hyperthermia: An Evaluation of the Potential for Localized Tissue Heating and Noninvasive Temperature Monitoring. *IEEE T Biomed Eng*. 1984;BME-31(1):161-167. doi:10.1109/TBME.1984.325382

2. Kuroda K. Non-invasive MR thermography using the water proton chemical shift. *Int J Hyperthermia*. 2005;21(6):547-560. doi:10.1080/02656730500204495

3. Quesson B, Zwart JA de, Moonen CTW. Magnetic resonance temperature imaging for guidance of thermotherapy. *J Magn Reson Imaging*. 2000;12(4):525-533. doi:10.1002/1522-2586(200010)12:4<525::AID-JMRI3>3.0.CO;2-V

4. Quesson B, Laurent C, Maclair G, et al. Real-time volumetric MRI thermometry of focused ultrasound ablation in vivo: a feasibility study in pig liver and kidney. *NMR Biomed*. 2011;24(2):145-153. doi:10.1002/nbm.1563

5. Ishihara Y, Calderon A, Watanabe H, et al. A precise and fast temperature mapping using water proton chemical shift. *Magn Reson Med*. 1995;34(6):814-823. doi:10.1002/mrm.1910340606

6. Sapareto SA, Dewey WC. Thermal dose determination in cancer therapy. *Int J Radiat Oncol Biol Phys*. 1984;10(6):787-800.

7. van Rhoon GC, Samaras T, Yarmolenko PS, Dewhirst MW, Neufeld E, Kuster N. CEM43°C thermal dose thresholds: a potential guide for magnetic resonance radiofrequency exposure levels? *Eur Radiol*. 2013;23(8):2215-2227. doi:10.1007/s00330-013-2825-y

8. Vappou J, Bour P, Marquet F, Ozenne V, Quesson B. MR-ARFI-based method for the quantitative measurement of tissue elasticity: application for monitoring HIFU therapy. *Phys Med Biol*. 2018;63(9):095018. doi:10.1088/1361-6560/aabd0d

9. Bitton RR, Webb TD, Pauly KB, Ghanouni P. Improving thermal dose accuracy in magnetic resonance-guided focused ultrasound surgery: Long-term thermometry using a prior baseline as a reference. *J Magn Reson Imaging*. 2016;43(1):181-189. doi:10.1002/jmri.24978

10. Rieke V, Pauly KB. Echo Combination to Reduce PRF Thermometry Errors From Fat. *J Magn Reson Imaging*. 2008;27(3):673-677. doi:10.1002/jmri.21238

11. Taylor BA, Elliott AM, Hwang K-P, Shetty A, Hazle JD, Stafford RJ. Measurement of temperature dependent changes in bone marrow using a rapid chemical shift imaging technique. *J Magn Reson Imaging*. 2011;33(5):1128-1135. doi:10.1002/jmri.22537

12. Soher BJ, Wyatt C, Reeder SB, MacFall JR. Noninvasive temperature mapping with MRI using chemical shift water-fat separation. *Magn Reson Med*. 2010;63(5):1238-1246. doi:10.1002/mrm.22310

13. Hofstetter LW, Yeo DTB, Dixon WT, Kempf JG, Davis CE, Foo TK. Fat-referenced MR thermometry in the breast and prostate using IDEAL. *J Magn Reson Imaging*. 2012;36(3):722-732. doi:10.1002/jmri.23692

14. Wu T, Felmlee JP, Greenleaf JF, Riederer SJ, Ehman RL. Assessment of thermal tissue ablation with MR elastography. *Magn Reson Med*. 2001;45(1):80-87. doi:10.1002/1522-2594(200101)45:1<80::AID-MRM1012>3.0.CO;2-Y

15. Mariani A, Kwiecinski W, Pernot M, et al. Real time shear waves elastography monitoring of thermal ablation: in vivo evaluation in pig livers. *J Surg Res*. 2014;188(1):37-43. doi:10.1016/j.jss.2013.12.024

16. Sapin-de Brosses E, Gennisson J-L, Pernot M, Fink M, Tanter M. Temperature dependence of the shear modulus of soft tissues assessed by ultrasound. *Phys Med Biol*. 2010;55(6):1701-1718. doi:10.1088/0031-9155/55/6/011

17. Chen J, Woodrum DA, Glaser KJ, Murphy MC, Gorny K, Ehman RL. Assessment of in vivo laser ablation using MR elastography with an inertial driver. *Magn Reson Med*. 2014;72(1):59-67. doi:10.1002/mrm.24891

18. Corbin N, Vappou J, Breton E, et al. Interventional MR elastography for MRI-guided percutaneous procedures. *Magn Reson Med*. 2016;75:1110-1118. doi:10.1002/mrm.25694

19. Hofstetter LW, Odéen H, Bolster BD, et al. Efficient shear wave elastography using transient acoustic radiation force excitations and MR displacement encoding. *Magn Reson Med*. 2019;81(5):3153-3167. doi:10.1002/mrm.27647

20. Tsao J, Jiang Y. Hierarchical IDEAL: Fast, robust, and multiresolution separation of multiple chemical species from multiple echo times. *Magn Reson Med*. 2013;70(1):155-159. doi:10.1002/mrm.24441

21. Yu H, Shimakawa A, McKenzie CA, Brodsky E, Brittain JH, Reeder SB. Multiecho water-fat separation and simultaneous R2* estimation with multifrequency fat spectrum modeling. *Magn Reson Med*. 2008;60(5):1122-1134. doi:10.1002/mrm.21737

22. Goldstein RM, Zebker HA, Werner CL. Satellite radar interferometry: Two-dimensional phase unwrapping. *Radio Sci*. 1988;23(4):713-720. doi:10.1029/RS023i004p00713

23. Le Y, Glaser K, Rouviere O, Ehman RL, Felmlee JP. Feasibility of simultaneous temperature and tissue stiffness detection by MRE. *Magn Reson Med*. 2006;55(3):700-705. doi:10.1002/mrm.20801

24. Manduca A, Muthupillai R, Rossman PJ, Greenleaf JF, Ehman RL. Image processing for magnetic-resonance elastography. In: *Medical Imaging 1996: Image Processing*. Vol 2710. International Society for Optics and Photonics; 1996:616-624. doi:https://doi.org/10.1117/12.237965

25. Manduca A, Lake DS, Kruse SA, Ehman RL. Spatio-temporal directional filtering for improved inversion of MR elastography images. *Med Image Anal*. 2003;7(4):465-473. doi:10.1016/S1361-8415(03)00038-0

26. Arnal B, Pernot M, Tanter M. Monitoring of thermal therapy based on shear modulus changes: II. Shear wave imaging of thermal lesions. *IEEE Trans Ultrason Ferroelectr Freq Control*. 2011;58(8):1603-1611. doi:10.1109/TUFFC.2011.1987

27. Sprinkhuizen SM, Konings MK, van der Bom MJ, Viergever MA, Bakker CJG, Bartels LW. Temperature-induced tissue susceptibility changes lead to significant temperature errors in PRFS-

based MR thermometry during thermal interventions. *Magn Reson Med*. 2010;64(5):1360-1372. doi:10.1002/mrm.22531

28. Shmatukha Andriy V., Harvey Paul R., Bakker Chris J.G. Correction of proton resonance frequency shift temperature maps for magnetic field disturbances using fat signal. *J Magn Reson Imaging*. 2007;25(3):579-587. doi:10.1002/jmri.20835

FIGURE CAPTIONS

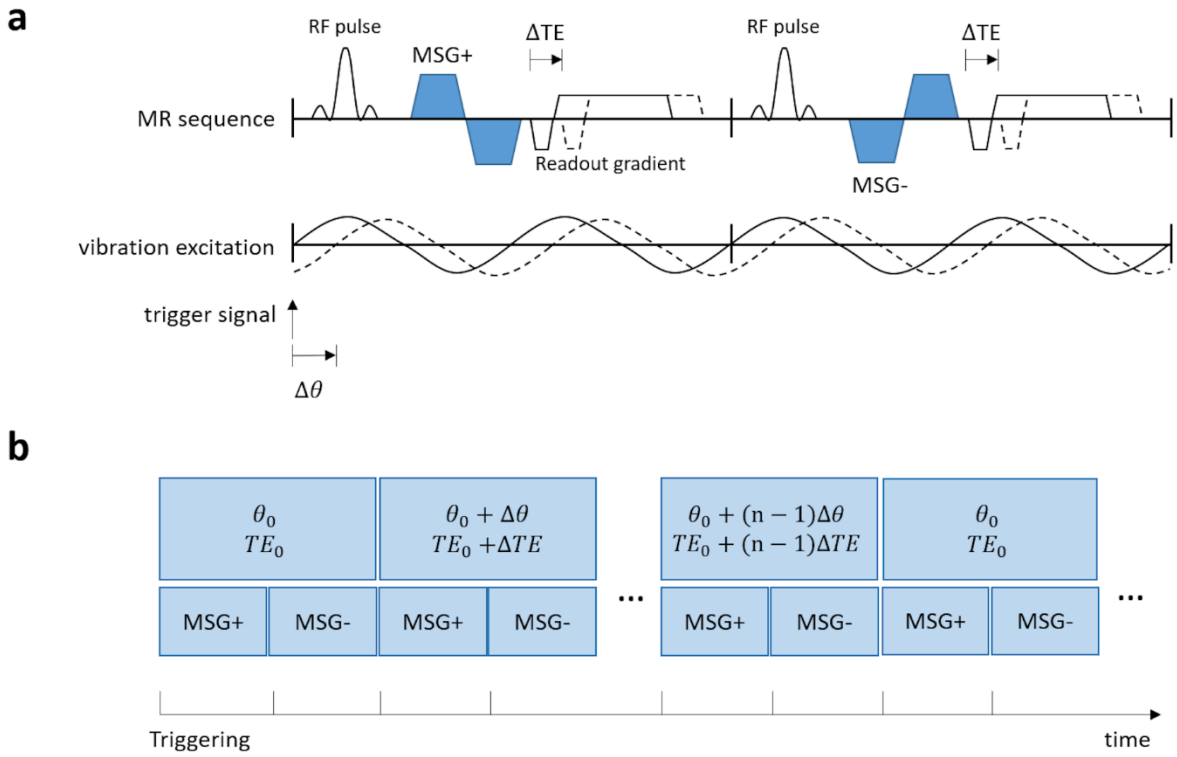

Figure 1. (a) Schematic chronogram of the GRE MRE sequence for simultaneous MRE and FRPRFS thermometry. For clarity, the main elements of the GRE MRE sequence are represented in a single line (RF pulse, MSG and read out gradient). TE and MRE phase-offsets are shifted by ΔTE and $\Delta\theta$, respectively. (b) Summarized acquisition scheme, with n being the number of phase-offsets and TEs. Images are acquired with alternating the polarity of MSG. Each pair of images is acquired with the same specific TE and phase-offset.

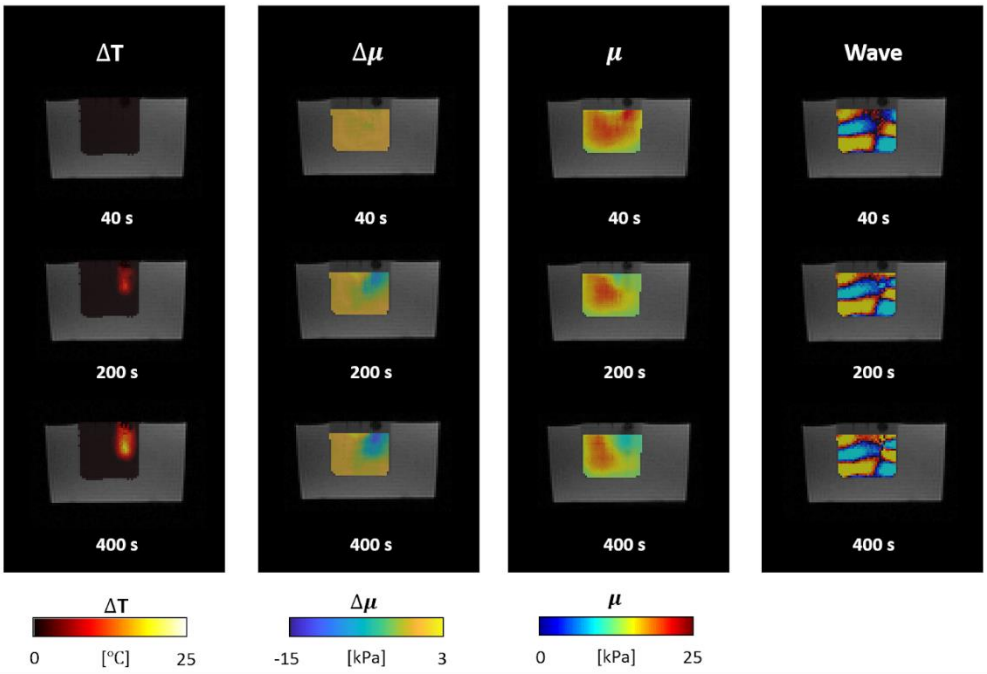

Figure 2. From left to right, temperature changes (ΔT), elasticity changes ($\Delta\mu$), elasticity maps (μ) and wave images overlaid with the magnitude image at the first TE, before (time 40 s) and during heating (times 200 s and 400 s). Localized increase in temperature result in gel softening in the inclusion.

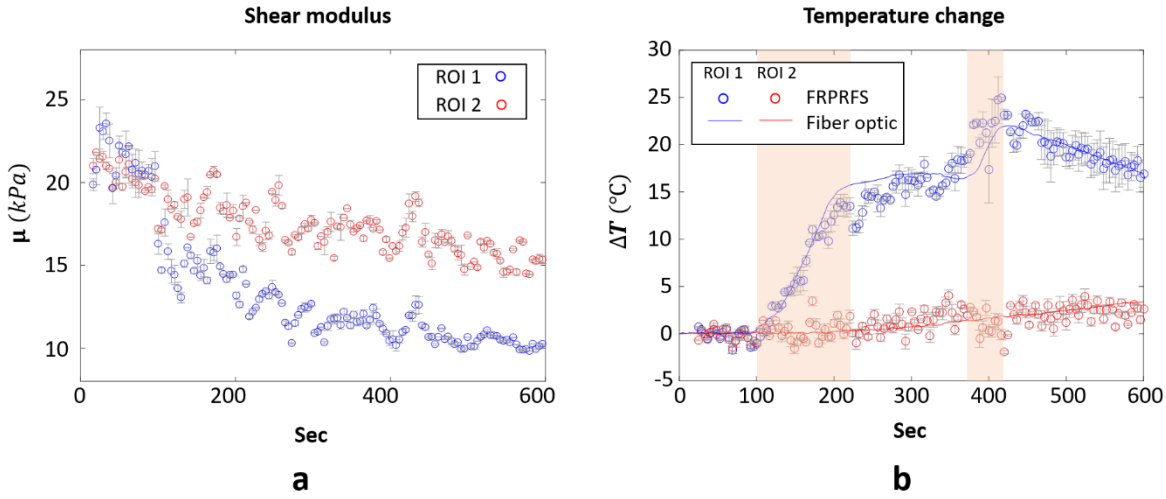

Figure 3. Time-dependent profiles of the shear modulus (a) and temperature changes ΔT (b) in ROI 1 and ROI 2 (2×2 pixels, shown in Fig. S1). Solid lines correspond to optical fiber thermometry (ROI 1 in blue, ROI 2 in red). Blue and red circles indicate measurements of the FRPRFS in ROI 1 and 2, respectively. The faded-orange regions in the graph indicate heating phases.

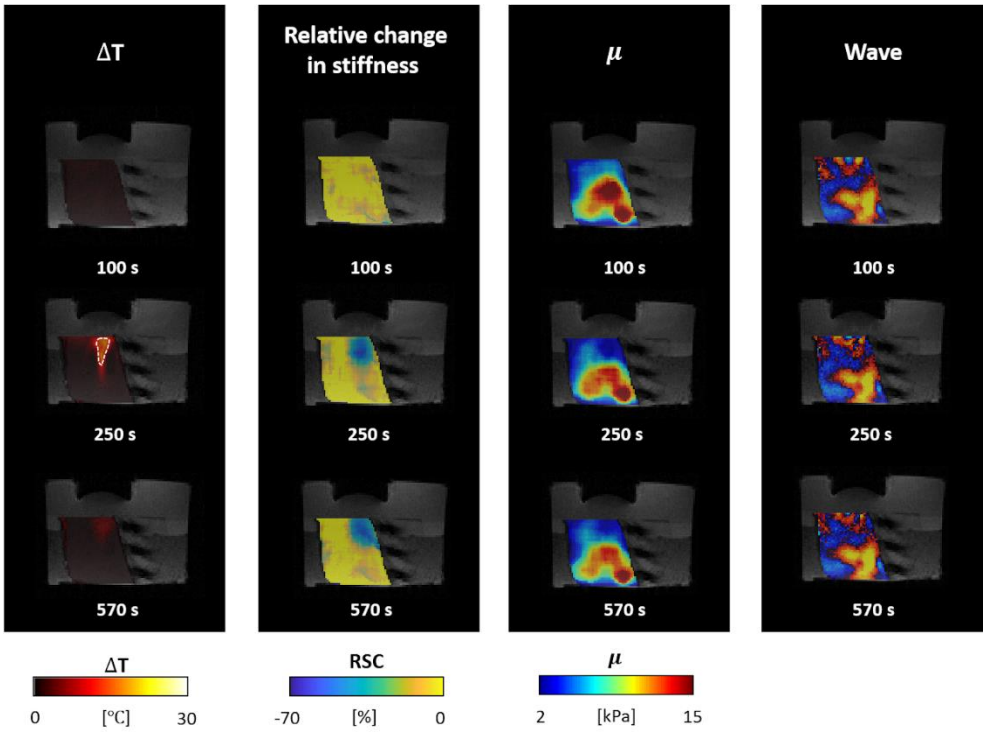

Figure 4. From left to right, temperature changes (ΔT), relative stiffness change (RSC), elasticity maps (μ), and wave images overlaid with the magnitude image at the first TE, before (time 100 s), during (time 250 s) the HIFU heating and after, during the cooling time (time 570 s) (Exp.#3). HIFU heating induces changes in the shear modulus (RSC).

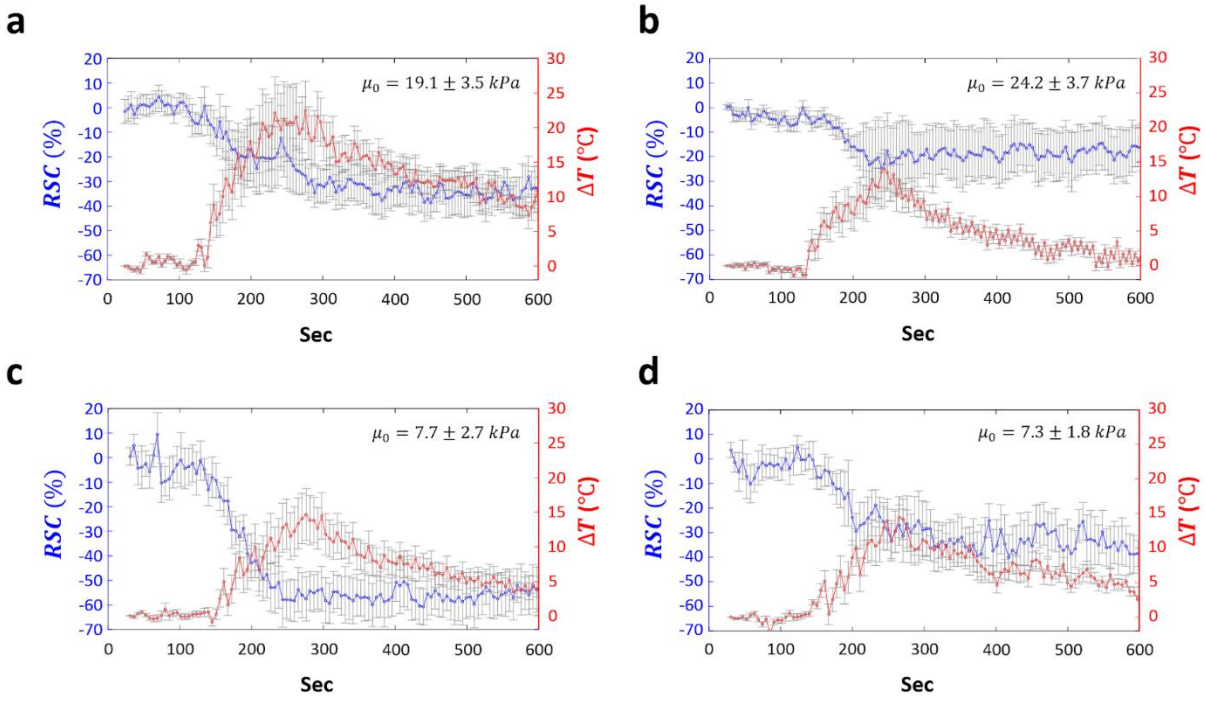

Figure 5. Time-dependent profiles of relative stiffness change (RSC) and temperature change ΔT in ex vivo muscle for Exp.#1 (a), #2 (b), #3 (c), and #4 (d). Mean initial elasticity value (μ_0) is given in the right top corner of each graph. ROIs were defined as the region including all pixels exceeding 66.7% of the maximum peak temperature increase around the focal spot (White-dashed line in Fig.4).

SUPPORTING INFORMATION

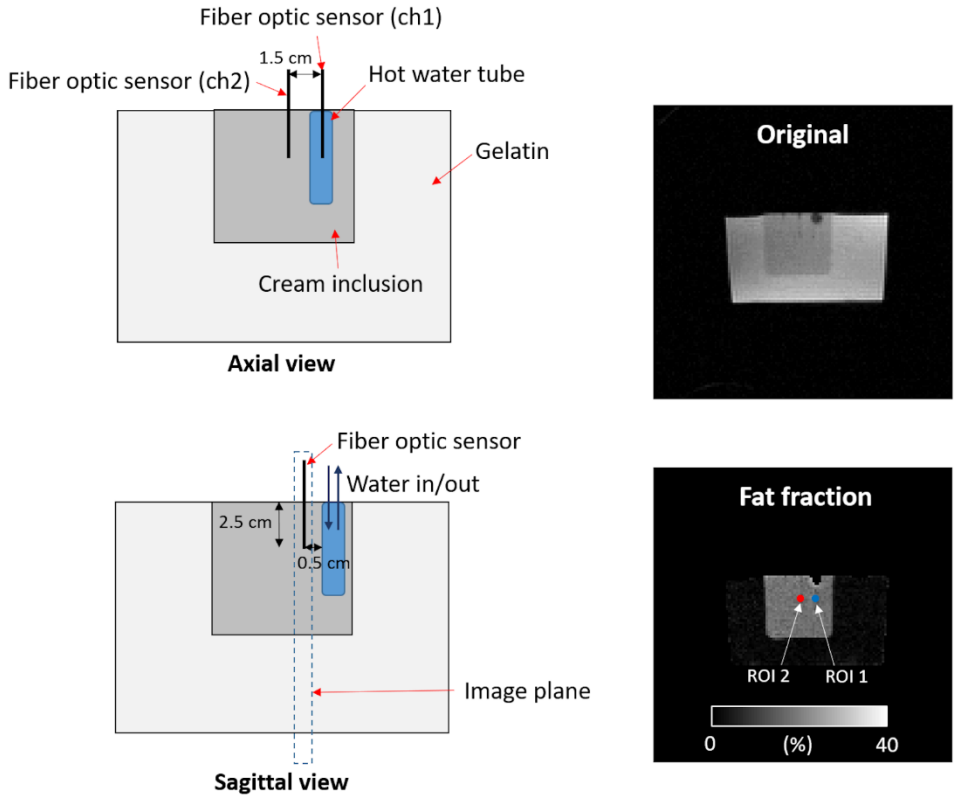

Figure S1. Schematic axial (top left) and sagittal views (bottom left) of the experimental setup, and the axial magnitude image (top right) and corresponding fat fraction map (bottom right) obtained before heating. The two optical fiber thermometers were positioned 15 mm apart in the image plane located 5 mm away from the hot tube side. A syringe was used for the manual circulation of hot water (about 90°C). The pneumatic exciter was placed below the phantom. ROI 1 and 2 indicate the position of the tips of the two optical fibers. A fat fraction value of 20.42±1.4% was measured before heating in the cream-gelatin inclusion, using the IDEAL algorithm; this result is consistent with the fat content of the cream (20% as provided by the manufacturer) used for this experiment.

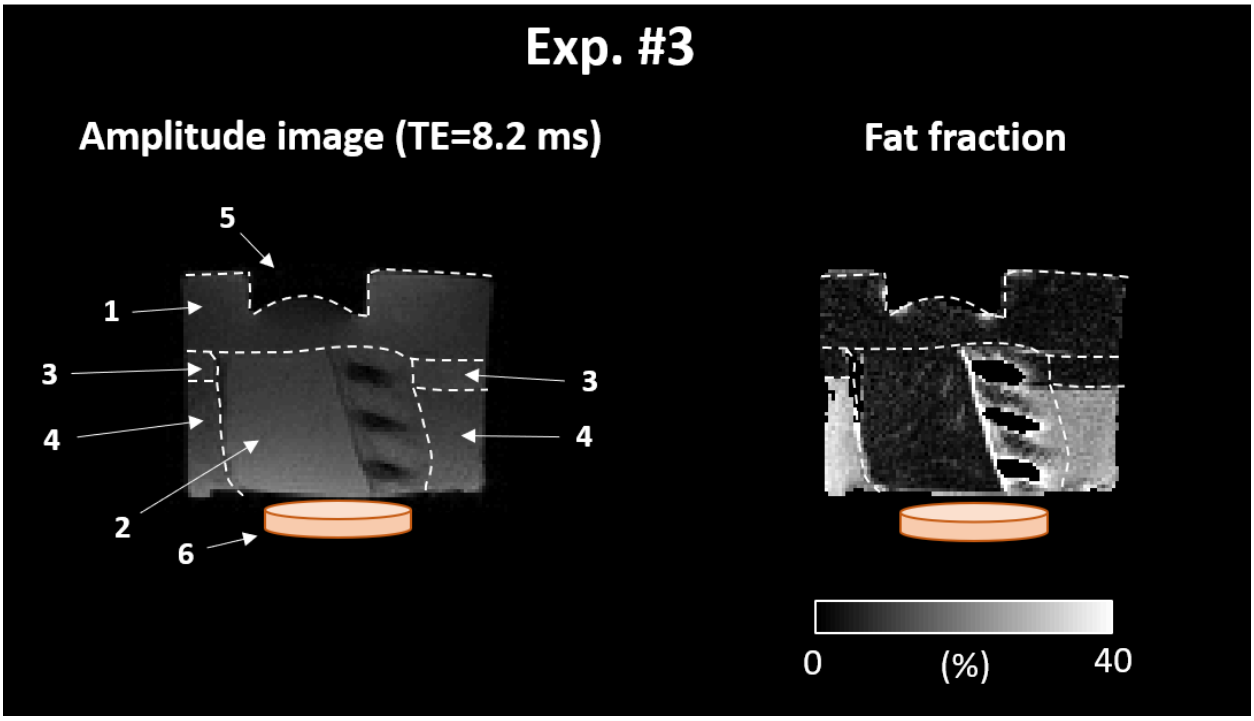

Figure S2. Experimental setup and fat fraction map before HIFU heating in ex vivo muscle. White-dashed lines delineate different areas of the phantom: -1- Degassed water, -2- Pig rib tissue, -3- 7% gelatin, -4- 2% gelatin in milk cream, -5- HIFU transducer, -6- Pneumatic exciter. Fat fractions were measured to be 5.7±3.3 % (muscle) and 22.2±1.5 % (cream gelatin).